CrystEngComm

PAPER

View Article Online
View Journal | View Issue

Cite this: *CrystEngComm*, 2019, **21**, 1934

Halogen and chalcogen-bonding interactions in sulphur-rich π-electron acceptors†

Yann Le Gal, Adrien Colas, Frédéric Barrière, Vincent Dorcet, Thierry Roisnel and Dominique Lorcy *

Received 30th November 2018,
Accepted 19th February 2019

DOI: 10.1039/c8ce02046a

rsc.li/crystengcomm

In order to explore the feasibility of generating halogen bonding interactions between sulphur-rich π-electron acceptors, we prepared three bithiazolidinylidene derivatives substituted by iodine atoms, namely 3,3′-bis(iodophenyl)bithiazolidinylidene-2,4,2′,4′-tetrathione (BIP-BTTT). Sulphur and iodine heteroatoms were introduced to the skeleton of the acceptor molecule to induce chalcogen···chalcogen and halogen bonding interactions. Both interactions can be evidenced by X-ray diffraction studies in the synthetic precursors as well as in the acceptors themselves.

Introduction

The design of molecules for the elaboration of semiconducting molecular materials relies essentially on the intrinsic properties of the molecular precursors. However, the properties of the materials are also based on the solid state organization and on the intermolecular interactions between molecules within the material.[1,2] Indeed, weak interactions between molecules will result in an insulating material with no charge carrier delocalization. Various types of intermolecular interactions have been explored such as chalcogen···chalcogen contacts,[3] hydrogen bonding,[4,5] π-π stacking,[6] and halogen bonding,[7] either separately or cooperatively.[8] In this context, we recently developed the synthesis of sulphur-rich electron acceptors with a bithiazolidinylidene-2,4,2′,4′-tetrathione (BTTT) backbone (Chart 1).[9]

Several members of this family led to air-stable *n*-channel organic field effect transistors (OFETs) exhibiting good performances.[10,11] The air stability and the enhanced charge mobility were ascribed to the presence of S···S intermolecular interactions.[10] As the intermolecular interactions are of high importance for the charge mobility as well as for the stability of *n*-channel OFETs,[12] we focused our interest on interactions other than chalcogen···chalcogen contacts. For this purpose, we investigated the synthesis of similar acceptors substituted with halogen atoms such as iodine, potentially able to form halogen bonds (XBs) with the chalcogen atoms of the neighbouring molecules, acting as XB acceptors. Indeed, we recently reported for example that the exocyclic sulphur atom in thiazoline-2-thiones can act as an efficient XB acceptor toward organic iodinated molecules.[13] Therefore we investigated the synthesis of 3,3′-bis(iodophenyl)-BTTT, BIP-BTTT (-Chart 1) where the nitrogen atoms of the heterocycles, the thiazoline-2-thione moieties, are substituted by an *ortho*, *meta* or *para* iodophenyl moiety. These different substitution patterns led to the analysis of the influence of the localization of the halogen atom on the intermolecular interactions. In this study, we report the syntheses and X-ray structure investigations of the precursors and the novel electron acceptors BIP-BTTT. Electrostatic surface potential (ESP) calculations carried out on four of the crystallographically characterized compounds provide a complementary understanding of the organization of the molecules in the solid state.

Results and discussion

The strategy we used to synthesize the acceptors BIP-BTTT **4a–c** starting from 2-, 3- and 4-iodoaniline is outlined in Scheme 1. Addition of triethylamine to a solution of the iodoaniline in carbon disulphide led to the dithiocarbamate salts **1a–c** in good yields. Alkylation of **1a–c** with chloroethanal followed by cyclization and dehydration in the presence of sulphuric acid allowed us to isolate the thiazoline-2-thiones **2a–c**. The next step involves the construction of the fused dithiole-2-one rings on the thiazoline-2-thiones **2a–c**. Successive addition of LDA and sulphur to thiazoline-2-thiones **2a–c**

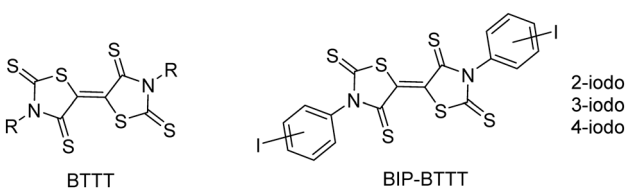

Chart 1

Univ Rennes, CNRS, ISCR (Institut des Sciences Chimiques de Rennes) - UMR 6226, F-35000 Rennes, France. E-mail: Dominique.lorcy@univ-rennes1.fr

† CCDC 1872721–1872724. For crystallographic data in CIF or other electronic format see DOI: 10.1039/c8ce02046a

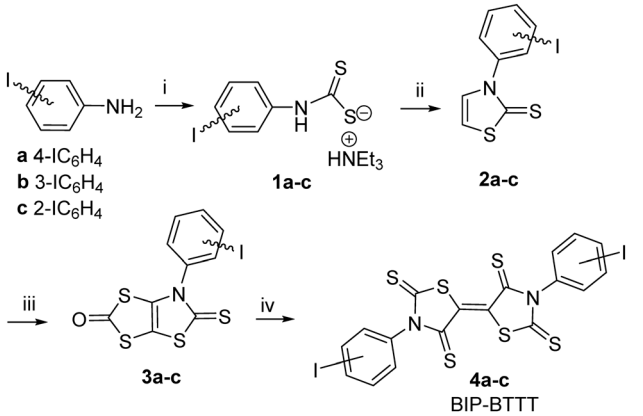

Scheme 1 Synthetic path to BIP-BTTT derivatives **4a–c**, 26–36% yield from **2a–c**. Reactants and conditions: i) CS_2, NEt_3; ii) $ClCH_2CHO$, H_2SO_4; iii) LDA, S_8, $(Cl_3CO)_2CO$; iv) toluene, Δ.

followed by the addition of triphosgene afforded the dithiol-2-ones **3a–c**. We previously demonstrated that a thermal treatment of such protected dithiolene ligands within a dithiol-2-one cycle is an efficient strategy for the synthesis of the acceptor skeleton.[9] The acceptors BIP-BTTT **4a–c** were therefore synthesized by simply heating the bicyclic structures **3a–c** in refluxing toluene. These acceptors **4a–c** were obtained as deep purple compounds poorly soluble in common organic solvents, the less soluble one being *para*-substituted **4a**.

Electrochemical investigations carried out by cyclic voltammetry allowed us to determine the redox potentials of these derivatives. They were performed in DMSO for the three acceptors **4a–c** and in CH_2Cl_2 only for **4b–c**, because **4a** is not soluble enough in dichloromethane. The redox potentials are collected in Table 1 together with those of DEBTTT (R = Et, Chart 1) for comparison. Two reversible monoelectronic reduction waves are observed for these three acceptors, either in DMSO or in CH_2Cl_2, attributed to the successive reduction of the acceptor into a radical anion and a dianion. Compared to DEBTTT, in both solvents the redox potentials of the acceptors **4a–c** are slightly shifted towards more anodic potentials, indicating a weak effect of the iodophenyl substituent on the overall accepting ability of these molecules. **4a–c** and DEBTTT exhibit slightly lower electron accepting ability than TCNQ (E_1 = 0.18 V and E_2 = −0.37 V *vs.* SCE).[14]

Crystals of sufficient quality for an X-ray diffraction study were obtained by slow concentration of a CH_2Cl_2 solution of **2b**, **3a** and **3c** as well as from a $CHCl_3$ solution of acceptor **4c**. The molecular structure of **2b** is reported in Fig. 1. The thiazole core is planar, while the phenyl ring is located in a plane forming a dihedral angle of 63.4(5)° with the thiazoline-2-thione core. The sulphur atoms can behave as a Lewis base and form intermolecular halogen bonding with the iodine atom of a neighbouring molecule.[13,15] However in **2b**, only a short distance between the hydrogen atom of the thiazoline ring and the sulphur atom of the thione (2.788(4) Å), assigned to a hydrogen bond (HB), was observed.

The molecular structures of dithiol-2-ones **3a** and **3c** are reported in Fig. 2. For both derivatives, the dithiol-2-one and the fused thiazoline core are coplanar and form with the plane of the aromatic substituent a dihedral angle of 50.5(2)° for **3a** and 100.2(3)° for **3c**. Short I···O contacts are observed between two neighbouring molecules of 3.271 Å for **3a** and 3.252 Å for **3c**, corresponding to a reduction ratio of 93.4% and 92.9% respectively, relative to the van der Waals contact distance (3.50 Å), indicating a sizeable XB interaction between neighbouring molecules (Fig. 2a and b).[16] The C–I···O angles, at 161.4° and 154.6°, are here closer to linearity and consistent with an XB interaction. In addition, for both structures, chalcogen···chalcogen contacts are also observed between neighboring molecules, at a distance shorter than the sum of the van der Waals radii, either between two sulphur centers (3.60 Å) or between sulphur and oxygen atoms (3.32 Å). The shortest sulphur···sulphur contacts measured for **3a** and **3c** are reported in Fig. 2c and d. The crystal structure of **3a** reveals S···O and S···S distances of 3.274(12) Å and 3.329(5) Å, respectively, the latter corresponds to 93% of the van der Waals distance and is due to strong noncovalent bonding between two molecules. Comparatively, the S···S distances within **3c** (the shortest being 3.416(1) Å) are longer than those in **3a**. This is ascribed to a steric effect in the solid state of the *ortho* position of the iodine atom on the phenyl ring.

Among the three electron acceptors, only the *ortho* substituted derivative **4c** could be analysed by X-ray diffraction. The molecular structure of this derivative is presented in Fig. 3. It crystallizes in the triclinic system, space group $P\bar{1}$, with two crystallographically independent molecules in the unit cell in general positions. This acceptor exhibits a

Table 1 Redox potentials $E_{1/2}$ V *vs.* SCE, in CH_2Cl_2 and DMSO for DEBTTT and **4a–c**

	CH_2Cl_2		DMSO	
Acceptors	$E_{1/2}{}^1$	$E_{1/2}{}^2$	$E_{1/2}{}^1$	$E_{1/2}{}^2$
DEBTTT	−0.05	−0.44	0.06	−0.41
4a			0.09	−0.33
4b	−0.01	−0.43	0.1	−0.34
4c	−0.04	−0.48	0.05	−0.37

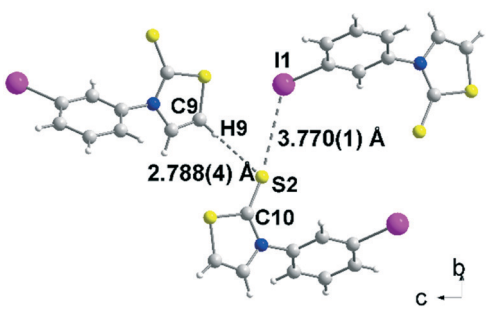

Fig. 1 View of the C–H···S= and C–I···S= interactions on the *bc* plane for **2b**.

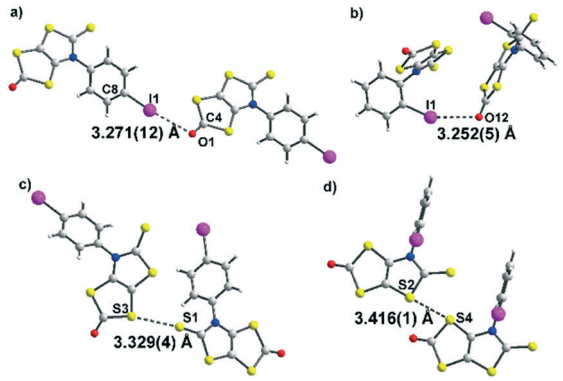

Fig. 2 View of the XB interactions; O···I contacts shorter than the sum of the van der Waals radii in dark grey dotted lines in **3a** (a) and **3c** (b). View of the chalcogen interactions; S···S contacts shorter than the sum of the van der Waals radii in dark grey dotted lines in **3a** (c) and **3c** (d).

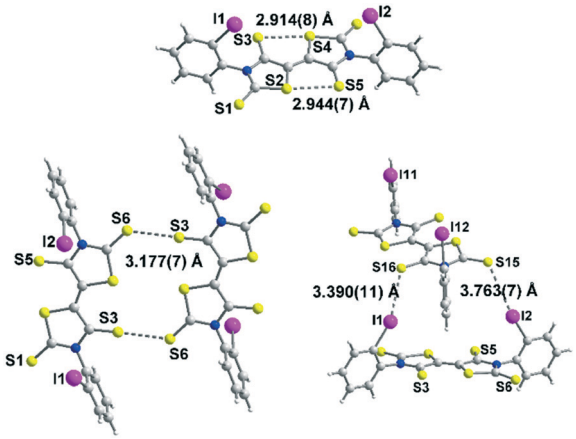

Fig. 3 Molecular structure of acceptor **4c** showing the intramolecular S···S contacts (top), the shortest intermolecular contacts (bottom left) and the XB bonds between two neighbouring molecules (bottom right).

planar skeleton and a *trans* configuration of the two thiazoline-2-thione rings with short intramolecular S···S contacts between the S atom of a thiocarbonyl group and the S atom of the thiazole ring (2.94 Å/2.91 Å). These short S···S contacts are in the same range as those observed for different acceptors belonging to the same family.[9]

Interestingly, the *ortho*-iodophenyl substituents on the nitrogen atoms have a similar orientation of the iodine pointing in the same direction above the plane of the acceptor. The plane of the phenyl rings is almost perpendicular to the plane of the acceptor. The molecules are associated through I···S=C XB interaction networks between $I_1\cdots S_{16}$ 3.390(4) Å and $I_{11}\cdots S_5$ 3.533(4) Å for the most significant short distances corresponding respectively to 89.7% and 93.4% of the van der Waals distances. Besides these intramolecular contacts, short S···S intermolecular contacts are also observed between neighbouring molecules, $S_3\cdots S_6$ 3.177(7) Å lower than the van der Waals radius of sulphur, corresponding to a reduction ratio of 88.2%. Nevertheless, due to steric hindrance generated by the iodophenyl rings, these S···S contacts within these acceptors are less numerous than those observed with DEBTTT where extensive three-dimensional S···S interactions were noticed.[10]

Electrostatic surface potential calculations have been performed on the optimized geometry of the four molecules that have been crystallographically characterized, namely **2b**, **3a**, **3c** and **4c**. These calculations were carried out in order to estimate the halogen bond donor abilities of the iodophenyl substituent within these different structures and to rationalize the interactions taking place in the crystals.[9] As shown in Fig. 4, for **2b** the maximum calculated positive electrostatic surface potential (ESP) is found at the hydrogen atoms located on the thiazole ring (+31.74 kcal mol^{-1}) compared to only +23.89 kcal mol^{-1} at the iodine atom. The most negative calculated ESP is −29.09 kcal mol^{-1} and located on the thione's sulphur atom (C=S). This calculated charge repartition is in good agreement with the organization of molecule **2b** in the solid state where predominant hydrogen bonding interactions were observed between the hydrogen atom on the thiazoline ring and the sulphur atom of the thione, while no specific halogen bonding interaction involving the iodine atom was detected.

For the dithiol-2-ones **3a** and **3c**, the most negative calculated ESP is now located on the oxygen atom of the dithiole rings (C=O, −19.92 and −25.14 kcal mol^{-1}, respectively), while the most positive ESP is on the bicyclic structure (+24.88 and +34.83 kcal mol^{-1}). The electrostatic surface potential value on the σ-hole of the halogen is lower (blue dot on the iodine atom in Fig. 4, +17.67 and +26.89 kcal mol^{-1}). Despite these slightly lower values, the organization of both molecules in the solid state shows XB interactions (C=O···I) between their iodine atom and the oxygen atom of a vicinal molecule.

Acceptor **4c** is the only example where the highest ESP value over the whole molecule is found at the σ-hole of the iodine atom (+24.48 kcal mol^{-1}, Fig. 4) while for the three

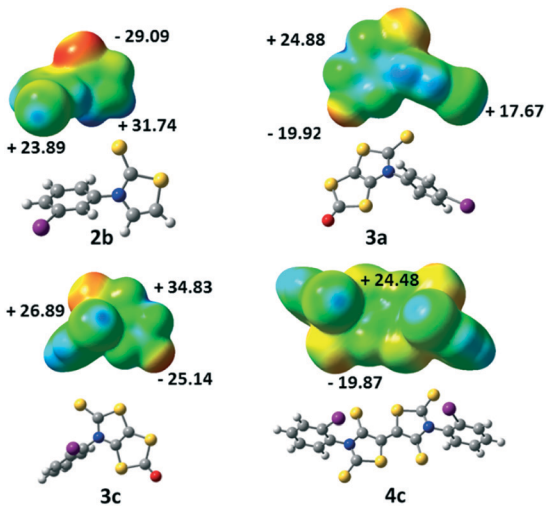

Fig. 4 Molecular electrostatic potential surface mapped at the 0.001 e^- au^{-3} isodensity surface for **2b**, **3a**, **3c** and **4c**. The common colour scale ranges from −29 kcal mol^{-1} (red) to +35 kcal mol^{-1} (blue).

Table 2 Relevant interatomic distances (Å) and angles (°) for the halogen bonding, hydrogen bonding and chalcogen interactions. The van der Waals contact distances amount to S···I: 3.78 Å, S···S: 3.60 Å, S···O: 3.32 Å, O···I: 3.50 Å, and H···S: 3.00 Å

	Distances (Å)	Angles (°)	
2b	$S_2\cdots H$ 2.788(4)	$C_9–H_9\cdots S_2$ 175.9(3)	$H_9\cdots S_2{=}C_{10}$ 98.4(2)
3a	$O_1\cdots I_1$ 3.271(12)	$C_8–I_1\cdots O_1$ 161.4(4)	$I_1\cdots O_1{=}C_4$ 109.2(8)
	$S_1\cdots S_3$ 3.329(4)		
3c	$O_{12}\cdots I_1$ 3.252(5)	$C_1–I_1\cdots O_{12}$ 154.6(9)	$I_1\cdots O_{12}{=}C_{11}$ 111.1(2)
	$S_2\cdots S_4$ 3.416(1)		
4c	$S_{15}\cdots I_2$ 3.763(7)	$C_{21}–I_2\cdots S_{15}$ 155.5(5)	$I_2\cdots S_{15}{=}C_{64}$ 118.7(6)
	$S_{16}\cdots I_1$ 3.390(4)	$C_1–I_1\cdots S_{16}$ 158.2(3)	$I_1\cdots S_{16}{=}C_{62}$ 119.4(6)
	$S_5\cdots I_{11}$ 3.533(4)	$C_{51}–I_{11}\cdots S_5$ 156.3(3)	$C_{12}{=}S_5\cdots I_{11}$ 124.9(5)
	$S_3\cdots S_6$ 3.177(7)		

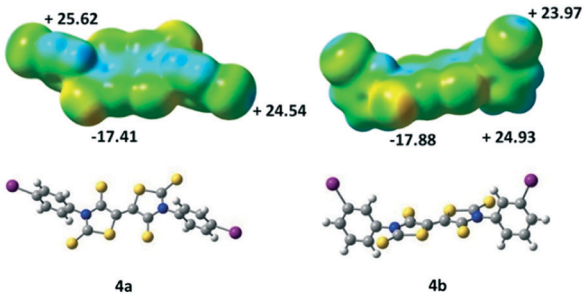

Fig. 5 Molecular electrostatic potential surface mapped at the 0.001 e^- au^{-3} isodensity surface for **4a** and **4b**. The colour scales range from −29 kcal mol^{-1} (red) to +35 kcal mol^{-1} (blue).

other derivatives, it was either found on a hydrogen atom for **2b** or on the bicycle structure for **3**. The most negative calculated ESP for **4c** is found on the sulphur atoms of the thione (−19.87 kcal mol^{-1}). In accordance with these calculations, the iodine atom of this acceptor is indeed involved in short XB interactions with the thione's sulphur atom in the solid state (Table 2).

We also performed some ESP calculations for the two other acceptors that have not been crystallographically characterized in order to analyse the influence of the localization of the halogen atom. For both acceptors, **4a** and **4b**, the most negative calculated ESP is located on the thione's sulphur atom (C═S) as with acceptor **4c**. On the other hand, the highest ESP value over the whole molecules **4a** and **4b** is not found at the σ-hole like for **4c** (Fig. 5) but located *para* to the iodine atom on the aromatic ring, potentially a less favorable charge distribution for the growth of crystals in these cases.

Conclusions

In this study we investigated the synthesis of sulphur-rich electron π-acceptors, bithiazolidinylidenes, substituted by iodophenyl substituents, which can act as halogen bond donors toward thione (C═S) or ketone (C═O) groups acting as XB acceptors. Single crystals of the synthetic intermediates as well as one of the acceptors have been obtained. For the precursors, when the thione (C═S) and ketone (C═O) groups are present on the molecule, a halogen bond is formed between the iodine atom of one molecule and the C═S/C═O moieties of the neighbouring ones. For acceptor **4c**, in accordance with the calculated ESP maxima, I···S═C halogen bonds are observed between neighbouring molecules as well as S···S interactions. Thus we managed to observe from these BIP-BTTT acceptors the coexistence of two types of intermolecular interactions in the solid state. The next step will be the design of sulphur-rich electron acceptors substituted by groups bearing an iodine atom but less bulky than phenyl in order to increase the strength of the intermolecular interactions.

Experimental section

All commercial chemicals were used without further purification. The solvents were purified and dried by standard methods. All the NMR spectra were obtained in $CDCl_3$ unless indicated otherwise. Chemical shifts are reported in ppm and ^1H NMR spectra were referenced to residual $CHCl_3$ (7.26 ppm) and ^{13}C NMR spectra were referenced to $CHCl_3$ (77.2 ppm). The ^{13}C NMR spectra of acceptors **4a–c** could not be obtained due to their low solubility. Melting points were measured on a Kofler hot-stage apparatus and are uncorrected. Mass spectrometry and elemental analyses were performed at the Centre Régional de Mesures Physiques de l'Ouest, Rennes. Cyclic voltammetry was carried out on a 10^{-3} M solution in CH_2Cl_2, containing 0.1 M nBu$_4$NPF$_6$ as the supporting electrolyte. Voltammograms were recorded at 0.1 Vs^{-1} on a platinum electrode and the potentials were measured *versus* the saturated calomel electrode (SCE).

N-Iodophenyl-1,3-thiazoline-2-thiones 2a–c

To a solution of 4-iodoaniline, 3-iodoaniline or 2-iodoaniline (12 g, 54.8 mmol) were added 100 mL of triethylamine and 100 mL of carbon disulphide. The solution was stirred under argon for 24 h. The solution was filtered and the yellow solid was washed with diethyl ether. The dithiocarbamate salts **1a–c** were used without further purification; **1a**: yield: 95%, Mp: 92 °C. ^1H NMR (300 MHz) δ 1.30 (t, 9H, ^3J = 7.3 Hz, CH_3), 3.17 (q, 6H, ^3J = 7.3 Hz, CH_2), 7.43 (m, 2H, Ar), 7.53 (m, 2H, Ar), 9.45 (s, 1H, NH); ^{13}C NMR (75 MHz) δ 8.8 (CH_3), 46.0 (CH_2), 88.2 (Ar), 125.2 (Ar), 137.7 (Ar), 140.8 (Ar), 214.3 (C═S); **1b**: yield: 97%; Mp: 100 °C; ^1H NMR (300 MHz) δ 1.36 (t, 9H, ^3J = 7.3 Hz, CH_3), 3.23 (q, 6H, ^3J = 7.3 Hz, CH_2), 6.99 (t, 1H, ^3J = 8.1 Hz, Ar), 7.39 (d, 1H, ^3J = 8.1 Hz, Ar), 7.62 (d, 1H, ^3J = 8.1 Hz, Ar), 8.10 (s, 1H, Ar), 9.40 (s, 1H, NH); ^{13}C NMR (75 MHz) δ 8.8 (CH_3), 46.0 (CH_2), 93.3 (Ar), 122.8 (Ar), 129.7 (Ar), 131.8(Ar), 133.3 (Ar), 142.1 (Ar), 214.7 (C═S); **1c**: yield: 92%; Mp: 95 °C; ^1H NMR (300 MHz) δ 1.36 (t, 9H, ^3J = 7.3 Hz, CH_3), 3.22 (q, 6H, ^3J = 7.3 Hz, CH_2), 6.85 (m, 1H, Ar), 7.31 (m, 1H, Ar), 7.78 (d, 1H, ^3J = 8.1 Hz, Ar), 8.08 (d, 1H, ^3J = 8.1 Hz, Ar), 9.02 (s, 1H, NH); ^{13}C NMR (75 MHz) δ 9.2 (CH_3); 46.0 (CH_2); 95.0 (Ar); 114.8 (Ar); 127.7 (Ar); 128.8 (Ar); 138.8 (Ar); 142.2 (Ar); 215.5 (C═S). To a solution of the dithiocarbamate salt (**1a–c**) (20.6 g, 52.0 mmol) was added 1 equivalent

of chloroacetaldehyde (0.96 mL, 52.0 mmol). The solution was stirred for 12 h at rt and 9/10 of the solvent was evaporated *in vacuo*. The mixture was added to 15 mL of H_2SO_4 at 0 °C and stirred for further 10 minutes. The solution was extracted with CH_2Cl_2 (3 × 50 mL), washed with water (3 × 20 mL) and dried over $MgSO_4$. The precipitate was washed with ethanol. Brown powders were obtained.

2a. Yield: 71%; Mp = 211 °C; ^{1}H NMR (300 MHz) δ 6.67 (d, 1H, ^3J = 4.7 Hz, SCH), 7.08 (d, 1H, ^3J = 4.7 Hz, NCH), 7.27 (d, 2H, ^3J = 4.7 Hz, Ar), 7.85 (d, 2H, ^3J = 4.7 Hz, Ar); ^{13}C NMR (75 MHz) 95.0 (Ar), 111.6 (C═C), 128.4 (2Ar), 132.1 (C═C), 138.3 (Ar), 138.9 (2Ar), 214.5 (C═S); HRMS (ESI) calcd for $C_9H_6INNaS_2$ $[M + Na]^+$: 341.88786. Found: 341.8882; anal calcd for $C_9H_6INS_2$: C, 33.87; H, 1.89; N, 4.39. Found: C, 33.68; H, 1.82; N, 4.38.

2b. Yield 87%; Mp: 119 °C; ^{1}H NMR (300 MHz) δ 6.68 (d, 1H, ^3J = 4.7 Hz, SCH), 7.10 (d, 1H, ^3J = 4.7 Hz, NCH), 7.24 (m, 1H, Ar), 7.51 (m, 1H, Ar), 7.80 (m, 2H, Ar), 7.83; ^{13}C NMR (75 MHz) δ 93.9 (Ar), 111.6 (C═C), 126.1 (C═C), 130.8 (Ar), 132.1 (Ar), 135.3 (Ar), 138.3 (Ar), 139.3 (Ar), 188.7 (C═S); HRMS (ESI) calcd for $C_9H_6INNaS_2$ $[M + Na]^+$: 341.88786. Found: 341.8881. Anal calcd for $C_9H_6INS_2$: C, 33.87; H, 1.89; N, 4.39. Found C, 33.51; H, 1.69; N, 4.42.

2c. Yield 72%; Mp:180 °C; ^{1}H NMR (300 MHz) δ 6.71 (d, 1H, ^3J = 4.7 Hz, SCH), 6.98 (d, 1H, ^3J = 4.7 Hz, NCH), 7.22 (m, 1H, Ar), 7.40 (m, 1H, Ar), 7.52 (m, 1H, Ar), 7.99 (m, 1H, Ar); ^{13}C NMR (75 MHz) δ 96.7 (Ar), 111.7 (C═C), 129.2 (C═C), 129.8 (Ar), 131.4 (2Ar), 140.4 (Ar), 141.5 (Ar), 189.0 (C═S); HRMS (ESI) calcd for $C_9H_6INNaS_2$ $[M + Na]^+$: 341.88786. Found 341.8877. Anal calcd for $C_9H_6INS_2$: C, 33.87; H, 1.89; N, 4.39. Found: C, 33.76; H, 1.69; N, 4.44.

Synthesis of bicycles 3a–c

To a −10 °C cooled solution of thiazoline (**2a–c**) (1 g, 3.12 mmol) in 80 mL of dry THF under nitrogen was added a solution of LDA prepared from diisopropylamine (0.66 ml, 4.8 mmol) and 1.6 M *n*-BuLi (2.93 mL, 4.8 mmol) in 10 mL of dry THF. After stirring for 30 min at −10 °C, sulphur S_8 (150 mg, 4.8 mmol) was added and the solution was stirred for an additional 30 min. A solution of LDA diisopropylamine (0.88 mL, 6.24 mmol) and *n*-BuLi (3.9 mL, 6.24 mmol) in 15 mL of dry THF was added. The mixture was stirred for 3 hours and S_8 (200 mg, 6.24 mmol) was added. After 30 min, triphosgene (1.11 g, 3.7 mmol) was added to the reaction mixture. The reaction was stirred overnight and water (15 mL) was slowly added. The solvent was evaporated *in vacuo*. Dichloromethane (50 mL) was added and the solution was washed with water (3 × 20 mL) and dried over $MgSO_4$. The concentrated solution was purified by chromatography on silica gel using CH_2Cl_2–petroleum ether as the eluent. Brown powders were obtained for **3a** and **3c**. **3b** was not isolated, and the crude oil was used without further purification.

3a. Yield: 36%; Mp = 174 °C; ^{1}H NMR (300 MHz) δ 7.20 (m, 2H, Ar); 7.92 (m, 2H, Ar). ^{13}C NMR ($CDCl_3$, 75 MHz) δ = 96.8 (Ar), 102.1 (C═C), 127.1 (C═C), 128.3 (2Ar), 137.2 (Ar), 139.6 (2Ar), 186.1 (C═S), 188.1 (C═O); IR $\nu_{(C=S)}$: 1261 cm^{-1}, $\nu_{(C=O)}$: 1695 cm^{-1}; HRMS (ESI) calcd for $C_{10}H_4INOS_4$ $[M + H]^+$: 409.82933. Found: 409.8296; anal. calcd for $C_{10}H_4INOS_4$: C, 29.34; H, 0.99; N, 3.42. Found: C, 29.68; H, 1.06; N, 3.50.

3c. Yield: 60%; Mp = 200 ° C; ^{1}H NMR (300 MHz) δ 7.29 (m, 1H, Ar), 7.44 (m, 1H, Ar), 7.58 (m, 1H, Ar), 8.02 (m, 1H, Ar); ^{13}C NMR (75 MHz) δ 94.2 (Ar), 108.1 (C═C), 112.6 (C═C), 131.1 (Ar), 131.7 (Ar), 138.8 (Ar), 139.4 (Ar), 143.7 (Ar), 191.6 (C═S), 192.1 (C═0); IR $\nu_{(C=S)}$: 1289 nm, IR $\nu_{(C=O)}$: 1660 nm; HRMS (ESI) calcd for $C_{10}H_4INOS_4$ $[M + H]^+$: 431.81127. Found: 431.8110; anal. calcd for $C_{10}H_4INOS_4$: C, 29.34; H, 0.99; N, 3.42. Found: C, 29.65; H, 0.92; N, 3.21.

Synthesis of BIP-BTTT 4a–c

A solution of thiazoline-thione **3a–c** (243 mg, 0.59 mmol) (crude compound for **3b**) in 30 mL of toluene was refluxed for 16 h. 80% of the solvent was removed *in vacuo* and the concentrated solution was filtered and the precipitate was washed with ethanol. Dark purple powders were obtained. Crystals of **4c** of sufficient quality for X-ray diffraction were obtained by slow evaporation of $CHCl_3$ solution.

4a. Yield: 72%, Mp > 250 °C; ^{1}H NMR (CS_2, 300 MHz) δ 7.08 (d, 4H, Ar), 7.89 (d, 4H, Ar); HRMS (ESI) calcd for $C_{18}H_9N_2IS_6$ $[M]^+$: 697.70958. Found 697.7101; UV-vis ($CHCl_2$) λ_{max} (nm) (ε [L mol^{-1} cm^{-1}]) = 242 (24 640), 358 (11 500), 520 (2550); anal. calcd for $[C_{18}H_8I_2N_2S_6$ + toluene (8/1)]: C, 31.93; H, 1.28; N, 3.95. Found: C, 32.08; H, 1.27; N, 3.95.

4b. Yield: 30% (calculated from **2b**), mp > 250 °C; ^{1}H NMR (CS_2, 300 MHz) δ 7.18 (m, 2H, Ar), 7.32 (m, 2H, Ar), 7.52 (m, 2H, Ar), 7.83 (m, 2H, Ar); UV-vis ($CHCl_2$) λ_{max} (nm) (ε [L mol^{-1} cm^{-1}]) = 232 (36 060), 359 (18 370), 512 (3420); HRMS (ESI) calcd for $C_{18}H_9N_2IS_6$ $[M + Na]^+$: 720.69935. Found 720.6993. Analysis calcd for $[C_{18}H_8I_2N_2S_6$ + toluene (8/1)]: C, 31.93; H, 1.28; N, 3.95. Found: C, 32.04; H, 1.32; N, 4.18.

4c. Yield: 60%, mp = 200 °C. ^{1}H NMR (300 MHz) δ 7.27 (m, 2H, Ar), 7.41 (m, 2H, Ar), 7.54 (m, 2H, Ar), 8.02 (m, 2H, Ar); UV-vis ($CHCl_2$) λ_{max} (nm) (ε [L mol^{-1} cm^{-1}]): 226 (28 670), 358 (14 928), 511 (2270); HRMS (ESI) calcd for $C_{18}H_9N_2IS_6$ $[M]^-$: 697.71068. Found: 697.7107; analysis calcd for $[C_{18}H_8I_2N_2S_6$ + toluene (8/1)]: C, 31.93; H, 1.28; N, 3.95. Found: C, 31.77; H, 1.25; N, 3.96.

Crystallography

Data were collected on a D8 VENTURE Bruker AXS diffractometer with graphite-monochromated Mo-Kα radiation (λ = 0.71073 Å) for **2b**, **3a**, **3c** and **4c**. The structures were solved by a dual-space algorithm using the *SHELXT* program,[17] and then refined with full-matrix least-squares methods based on F^2 (*SHELXL*).[18] All non-hydrogen atoms were refined with anisotropic atomic displacement parameters. H atoms were finally included in their calculated positions. Concerning **3a**, the use of the Platon/TwinRotMat[19] routine allowed the presence of a twinning in the measured crystal to be detected. Satisfactory final structural refinement has been performed considering the presence of such a twinning and in the hklf5

Table 3 Crystallographic data

Compound	2b	3a	3c	4c
Formula	$C_9H_6INS_2$	$C_{10}H_4INOS_4$	$C_{10}H_4INOS_4$	$C_{18}H_8I_2N_2S_6$
FW (g mol^{-1})	319.17	409.28	409.28	698.42
Crystal system	Monoclinic	Monoclinic	Monoclinic	Triclinic
Space group	$C2/c$	$P2_1/n$	$P2_1/c$	$P\bar{1}$
a (Å)	8.7777(10)	4.1078(7)	8.1394(7)	12.5260(18)
b (Å)	11.1568(15)	24.675(5)	6.9798(7)	14.352(2)
c (Å)	21.241(3)	13.943(3)	22.487(2)	14.522(2)
α (°)	90	90	90	117.141(4)
β (°)	96.632(4)	118.785(7)	94.788(3)	95.478(5)
γ (°)	90	90	90	100.638(5)
V (Å^3)	2066.3(5)	1238.6(4)	1273.1(2)	2234.7(6)
T (K)	150(2)	150(2)	150(2)	150(2)
Z	8	4	4	4
D_{calc} (g cm^{-3})	2.052	2.195	2.135	2.076
μ (mm^{-1})	3.454	3.238	3.151	3.384
Total refls.	8223	11 687	14 751	51 086
Abs. corr.	Multi-scan	Multi-scan	Multi-scan	Multi-scan
Uniq. refls. (R_{int})	2344 (0.0274)	—	2904 (0.0404)	10 225 (0.1050)
Uniq. refls. ($I > 2\sigma(I)$)	2188	8472	2675	6098
R_1, wR_2	0.0307, 0.0974	0.0758, 0.1622	0.0306, 0.0814	0.1160, 0.3164
R_1, wR_2 (all data)	0.0336, 0.1095	0.1094, 0.1758	0.0337, 0.0834	0.1793, 0.3626
GoF	1.101	1.042	1.054	1.079

file format, leading to a refined twin ratio of 0.19. Crystallographic data on X-ray data collection and structure refinements are given in Table 3.

Theoretical modeling

Electrostatic surface potential calculations were carried out on the optimized geometry of the molecules (with density functional theory using the Gaussian 09 revision D.01 software, the B3LYP functional and the 6-31+G** basis set for all the atoms and the LANLdp basis set for iodine). GaussView 5.0.9 was used to generate the figures.

Conflicts of interest

There are no conflicts to declare.

Notes and references

1 S. Sutton, C. Risko and J. L. Brédas, *Chem. Mater.*, 2016, **28**, 3–16.
2 G. R. Desiraju, *J. Am. Chem. Soc.*, 2013, **135**, 9952–9967.
3 R. Gleiter, G. Haberhauer, D. B. Werz, F. Rominger and C. Bleiholder, *Chem. Rev.*, 2018, **118**, 2010–2041.
4 G. R. Desiraju, *Cryst. Growth Des.*, 2011, **11**, 896–898.
5 E. D. Głowacki, M. Irimia-Vladu, S. Bauer and N. S. Sariciftci, *J. Mater. Chem. B*, 2013, **1**, 3742–3753.
6 K. S. Kim, P. Tarakeshwar and J. Y. Lee, *Chem. Rev.*, 2000, **100**, 4145–4185.
7 (*a*) G. Cavallo, P. Metrangolo, R. Milani, T. Pilati, A. Priimagi, G. Resnati and G. Terraneo, *Chem. Rev.*, 2016, **116**, 2478–2601; (*b*) L. C. Gilday, S. W. Robinson, T. A. Barendt, M. J. Langton, B. R. Mullaney and P. D. Beer, *Chem. Rev.*, 2015, **115**, 7118–7195.
8 A. S. Mahadevi and G. N. Sastry, *Chem. Rev.*, 2016, **116**, 2775–2825.
9 (*a*) Y. Le Gal, N. Bellec, F. Barrière, R. Clérac, M. Fourmigué, V. Dorcet, T. Roisnel and D. Lorcy, *Dalton Trans.*, 2013, **42**, 16672–16679; (*b*) Y. Le Gal, D. Ameline, N. Bellec, A. Vacher, T. Roisnel, V. Dorcet, O. Jeannin and D. Lorcy, *Org. Biomol. Chem.*, 2015, **13**, 8479–8486; (*c*) Y. Le Gal, M. Rajkumar, A. Vacher, V. Dorcet, T. Roisnel, M. Fourmigué, F. Barrière, T. Guizouarn and D. Lorcy, *CrystEngComm*, 2016, **18**, 3925–3933.
10 A. Filatre-Furcate, T. Higashino, D. Lorcy and T. Mori, *J. Mater. Chem. C*, 2015, **3**, 3569–3573.
11 (*a*) K. Iijima, Y. Le Gal, T. Higashino, D. Lorcy and T. Mori, *J. Mater. Chem. C*, 2017, **5**, 9121–9127; (*b*) K. Iijima, Y. Le Gal, D. Lorcy and T. Mori, *RSC Adv.*, 2018, **8**, 18400–18405.
12 C. Wang, H. Dong, W. Hu, Y. Liu and D. Zhu, *Chem. Rev.*, 2012, **112**, 2208–2267.
13 Y. Le Gal, D. Lorcy, O. Jeannin, F. Barrière, V. Dorcet, J. Lieffrig and M. Fourmigué, *CrystEngComm*, 2016, **18**, 5474–5481.
14 M. L. Kaplan, R. C. Haddon, F. B. Bramwell, F. Wudl, J. H. Marshall, D. O. Cowan and S. Gronowitz, *J. Phys. Chem.*, 1980, **84**, 427–431.
15 M. Arca, M. C. Aragoni, F. A. Devillanova, A. Garau, F. Isaia, V. Lippolis, A. Mancini and G. Verani, *Bioinorg. Chem. Appl.*, 2006, 58937.
16 P. Auffinger, F. A. Hays, E. Westhof and P. S. Ho, *Proc. Natl. Acad. Sci. U. S. A.*, 2004, **101**, 16789–16794.
17 G. M. Sheldrick, *Acta Crystallogr., Sect. A: Found. Adv.*, 2015, **71**, 3–8.
18 G. M. Sheldrick, *Acta Crystallogr., Sect. C: Struct. Chem.*, 2015, **71**, 3–8.
19 A. L. Spek, *Acta Crystallogr., Sect. A: Found. Crystallogr.*, 1990, **46**, C34.